Journal of Electrostatics 87 (2017) 243–250

Contents lists available at ScienceDirect

Journal of Electrostatics

journal homepage: www.elsevier.com/locate/elstat

Charge and size of a ring in an electrolyte with atomic force microscopy

Daniel Lazarev, Fredy R. Zypman*

Yeshiva University, New York, NY 10033, USA

ARTICLE INFO

Article history:
Received 30 March 2017
Received in revised form
9 May 2017
Accepted 11 May 2017
Available online 23 May 2017

ABSTRACT

We study the interaction force between a ring with a dipole density and the tip of an Atomic Force Microscope. Given the vector nature of a dipole we study the force for all possible dipole orientations. These results are applied to the practical problem of a charged ring electrically partially shielded by ions in an electrolyte. We provide theoretical tools to analyze experiments and extract parameters such as the charge and size of the ring, the screening, and the Debye length.

1. Introduction

An object embedded in an electrolyte has its charge shielded by the counterions in solution. Thus, any instrument aimed at measuring the charge of the object must account for the electrostatic problem that includes the embedding electrolyte. Here we are interested in understanding the response of the Atomic Force Microscope (AFM) to a charged ring immersed in an electrolyte, a ubiquitous case in soft matter in which all or part of the ring's charge is shielded by the ions in the medium [1–3]. The problem of how to use the AFM to measure size and charge of nano-rings in air has already been solved [4]. This work extends that result to the most relevant case of the AFM with fluid cells [5–7]. Thus the methods developed in this article should be of use to measure static charge in liquid. This liquid could be of explicit interest such as is the case in electrochemistry or in biological buffers, but also due to its implicit presence as humidity when nominally making measurements in air. From a fundamental electrostatic standpoint, we obtain for the first time the electrostatic field produced by the interaction of the ring of charge with the liquid and the spherical tip of the AFM.

We first consider two rings of opposite charges characterized by an electric dipole density. We analyze two specific configurations for oppositely charged near rings—one *stacked*, in which one ring is vertically above the other, and the second *concentric,* with one ring inside the other on the same horizontal plane. We further show that the electric field produced by a system comprised of two oppositely charged near rings of arbitrary orientation can always be treated as a linear combination of the stacked and concentric cases.

Integrating over all such orientations we obtain the AFM forces for a bare charged ring dressed by ionic charge. Since in a practical situation this dressing generally produces partial screening, the total force on the AFM is obtained as the sum of the force produced by a bare ring of charge and that produced by a dipole ring of charge, modulated by a parameter representing the particular ionic conditions of the surrounding electrolyte.

A note on notation used: Since the experimental quantity accessible in AFM is the vertical force on the tip, the electric field and force expressions we consider in this paper are all in the z-direction. To simplify the notation, we will not write the subscript "z." In addition, the stacked case quantities are labeled '$\boxminus$,' while the concentric case quantities are indicated by '$\odot$.'

The paper is organized as follows. In section 2, Theory, we briefly review, in subsection 2.1, the case of a single charged ring as it is necessary to introduce notation. Subsections 2.2 and 2.3 already get into the systems focus of this paper, the stacked and concentric ring configurations. Section 3 presents the derivation of forces for both cases mentioned above. Subsection 3.3 shows a proof that a force in a generic configuration can always be written as a linear combination of the cases studied in section 3. Section 4 is an application of the results for the case of a ring embedded in an electrolyte. Section 5 shows how in practice to obtain dipole and size of the ring from the AFM force measurements. Section 6 presents experiments that have used AFM to study ring structures ranging in size from $\mathring{A}$ to microns. 7 is the conclusion section.

* Corresponding author.
E-mail address: zypman@yu.edu (F.R. Zypman).

http://dx.doi.org/10.1016/j.elstat.2017.05.004
0304-3886/

2. Theory

2.1. Charged ring

In this subsection we briefly state the results for electric field and AFM force generated by a ring of charge. This problem has already been solved [4], but we succinctly show the salient features of that analysis to introduce notation and relevant results needed for this article.

For a single ring of radius A and total charge Q, the electric field in the z-direction at $(x,\ 0, z)$ is given by

$$E(A,x,z) = \frac{Q}{(2\pi)^2\varepsilon}\frac{z}{\left(x^2+z^2+A^2\right)^{\frac{3}{2}}} f[\mu(A,x,z)], \tag{1}$$

where μ and $f(\mu)$ are defined by

$$\mu = \frac{2Ax}{x^2+z^2+A^2} \tag{2}$$

$$f(\mu) = -\frac{2\mathbb{E}\left(\frac{2\mu}{1+\mu}\right)}{(\mu-1)\sqrt{1+\mu}}, \tag{3}$$

with $\mathbb{E}(m)$ the Elliptic Integral of the Second Kind [8], and ε the medium's permittivity [9]. To find the force on the AFM tip with radius of curvature R (Fig. 1) due to the ring, we evaluate the electric field at a point on the image ring, $x = B = \frac{AR^2}{A^2+d^2}$ and $z = d - d' = d - \frac{R^2}{A^2+d^2}d$, multiply by 2π to obtain the total field acting on the image ring, and finally multiply by the image charge, which gives:

$$F^0 = -F_0\frac{\eta\beta^2}{\sqrt{\beta^2+\eta^2}}\left\{\frac{1-\frac{1}{\beta^2+\eta^2}}{\left[\beta^2+\left(\frac{\beta}{\beta^2+\eta^2}\right)^2+\left(\eta-\frac{\eta}{\beta^2+\eta^2}\right)^2\right]^{\frac{3}{2}}}\right\} f(\mu), \tag{4}$$

where $\eta \equiv \frac{d}{R}$, $\beta \equiv \frac{A}{R}$, and $F_0 \equiv \frac{\lambda^2}{\varepsilon_0}$, λ being the linear charge density on the ring. F^0 is then the force corresponding to zero ion concentration. For the two-ring systems described in the Introduction, Equation (1) will be the starting point.

2.2. Stacked ring configuration

This geometry corresponds to two near rings of equal diameters exactly above each other (Fig. 2). Taking ring 1 (red) in Fig. 2 to be positive, and ring 2 (blue) negative, the electric field due to the former is $E^+_{\boxminus} = E(A,\ x,\ z)$, while the field due to the latter is $E^-_{\boxminus} = -E(A,\ x,\ z - L_{\boxminus})$, where the function E is defined in Equation (1).

The total vertical electric field at a point $P = (x,\ 0,\ z)$ is $E_{\boxminus} = E^+_{\boxminus} + E^-_{\boxminus}$. Expanding this expression as a power series in $L_{\boxminus}$, and keeping terms to first order in $L_{\boxminus}$, gives

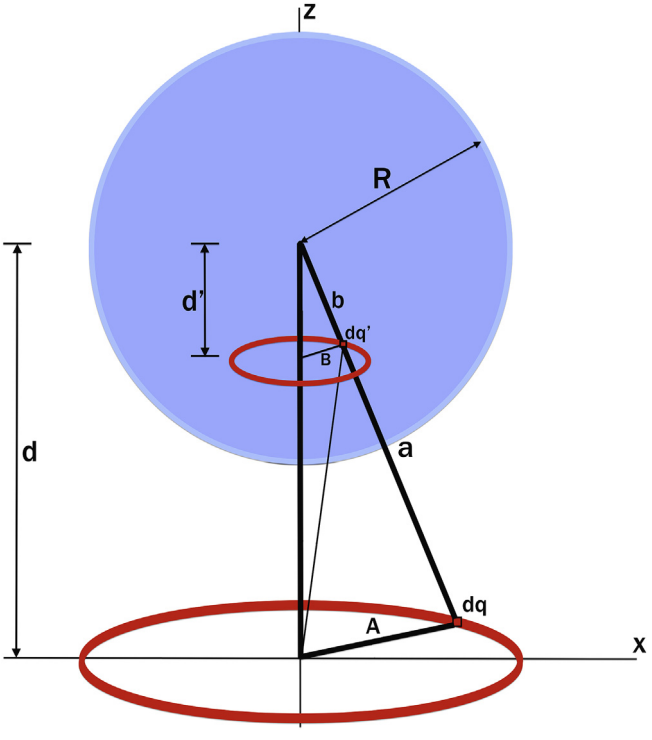

Fig. 1. A ring of radius A near an AFM tip with radius of curvature R produces an image ring of radius B.

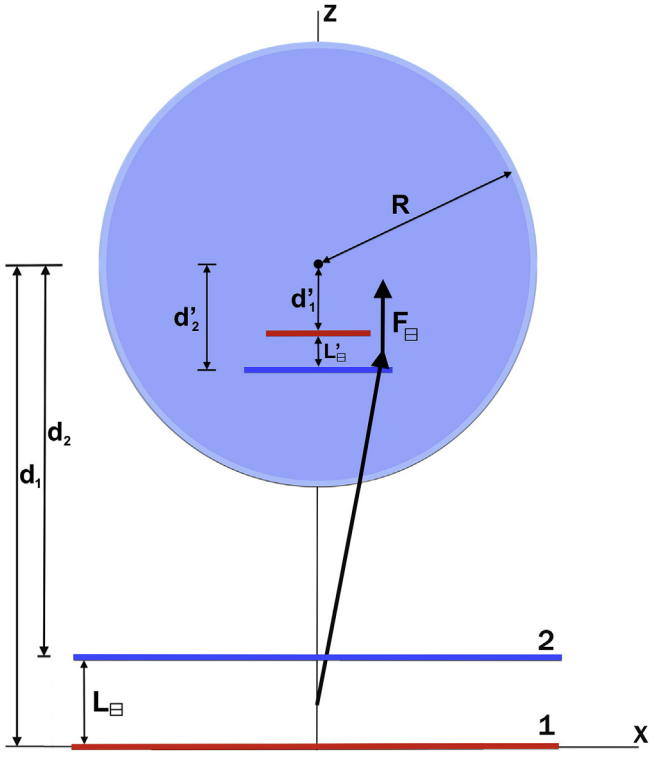

Fig. 2. Sagittal view of the stacked ring setup near an AFM tip, and the resulting image rings. The lines labeled "1" and "2" are rings of opposite charge, lying on the horizontal plane. The image rings inside the sphere are shown with slightly different radii, but in the limit $L_{\boxminus} \to 0$ they overlap.

$$E_{\boxminus} = \frac{QL_{\boxminus}}{(2\pi)^2\varepsilon}\left\{\frac{2\left[\left(A^6+2A^5x-A^4x^2+x^6-3x^2z^4-2z^6-4A^3x\left(x^2+z^2\right)-A^2\left(x^4+8x^2z^2+3z^4\right)+2A\left(x^5-2x^3z^2-3xz^4\right)\right]\mathbb{E}(m_1)}{\sqrt{A^2+x^2+z^2}\left(A^2-2Ax+x^2+z^2\right)^2\left(A^2+2Ax+x^2+z^2\right)^2\sqrt{1+\frac{2Ax}{A^2+x^2+z^2}}}\right.$$
$$\left.+\frac{\pi Axz^2\left(A^2-2Ax+x^2+z^2\right){}_2F_1\left(\frac{1}{2},\frac{3}{2},2,m_1\right)}{\sqrt{A^2+x^2+z^2}\left(A^2-2Ax+x^2+z^2\right)^2\left(A^2+2Ax+x^2+z^2\right)^2\sqrt{1+\frac{2Ax}{A^2+x^2+z^2}}}\right\} \tag{5}$$

where $m_1 = \frac{4Ax}{A^2+2Ax+x^2+z^2}$, and ${}_2F_1$ is the hypergeometric function [10]. By defining the constant $E_{0,\boxminus} \equiv \frac{QL_{\boxminus}}{(2\pi)^2\varepsilon R^3}$, which carries the units of electric field, we express the rest of the expression in terms of dimensionless parameters $\tilde{x} = x/R$ and $\tilde{z} = z/R$. Equation (5) can then be written as $E_{\boxminus}(x, z) = E_{0,\boxminus}\tilde{E}_{\boxminus}(\tilde{x}, \tilde{z})$, where we have appended a tilde to denote the dimensionless component of the corresponding expression for the electric field. In Appendix 1 in the Supplementary Material we give explanation for the flipping of the order of the image rings and the conservation of electric dipole directionality for the image rings, as portrayed in Fig. 2.

2.3. Concentric ring configuration

In this configuration, two rings lie on the same horizontal plane, with one of the rings inside the other (Fig. 3). The electric field due to the positively charged ring is, as in the previous sub-section, $E^+_{\odot} = E(A, x, z)$. The electric field of the outer ring is $E^-_{\odot} = -E(A + L_{\odot}, x, z)$.

The total electric field on point $P = (x, z)$ is $E_{\odot} = E^+_{\odot} + E^-_{\odot}$. Expanding this expression as a power series to first order in $L_{\odot}$, we obtain

3. Forces

3.1. Force for the stacked case

Having determined the electric fields, we can now calculate the force on the AFM tip. The force in the z-direction acting on the dipole image rings is the product of the total image charge and the electric field acting on it, $E_{\boxminus}$. The electric field acting on the negative image ring (blue inside sphere in Fig. 2) is $-E_{\boxminus}$, while that acting on the positive one (red inside sphere in Fig. 2) is $+(E_{\boxminus} + dE_{\boxminus})$, where $dE_{\boxminus}$ is the change in the electric field over the distance $L'_{\boxminus}$. Summed up, only $+dE_{\boxminus}$ is left, so we have:

$$F_{\boxminus} = Q' dE_{\boxminus}. \tag{7}$$

Multiplying and dividing by the small distance element $dz = L'_{\boxminus}$, over which the electric field is changing, we obtain [11]

$$F_{\boxminus} = Q'\frac{\partial E_{\boxminus}}{\partial z}dz = Q'L'_{\boxminus}\frac{\partial E_{\boxminus}}{\partial z}. \tag{8}$$

After taking the derivative, $\frac{\partial E_{\boxminus}}{\partial z}$ has an extra length dimension in the denominator, so the unit-carrying constant is now $\frac{E_{0,\boxminus}}{R} = \frac{QL_{\boxminus}}{(2\pi)^2\varepsilon R^4}$.

$$E_{\odot} = \frac{QL_{\odot}}{(2\pi)^2\varepsilon}z\left\{\frac{2\left(A^2+x^2+z^2+2Ax\right)\left[A^6+6A^5x+A^4\left(z^2-5x^2\right)-\left(z^2+x^2\right)^3+6A^3\left(x^3-xz^2\right)+A^2\left(5x^4+4x^2z^2-z^4\right)\right]\mathbb{E}(m_1)}{A\left(A^2+x^2+z^2\right)^{\frac{3}{2}}\left(A^2-2Ax+x^2+z^2\right)^2\left(A^2+2Ax+x^2+z^2\right)^2\sqrt{1+\frac{2Ax}{A^2+x^2+z^2}}}\right.$$
$$\left.+\frac{A^2\pi\left(A^2-x^2+z^2\right)\left(A^2+x^2+z^2\right)\left(A^2-2Ax+x^2+z^2\right){}_2F_1\left(\frac{1}{2},\frac{3}{2},2,m_1\right)}{A\left(A^2+x^2+z^2\right)^{\frac{3}{2}}\left(A^2-2Ax+x^2+z^2\right)^2\left(A^2+2Ax+x^2+z^2\right)^2\sqrt{1+\frac{2Ax}{A^2+x^2+z^2}}}\right\} \tag{6}$$

Define $E_{0,\odot} \equiv \frac{QL_{\odot}}{(2\pi)^2\varepsilon R^3}$ to write Equation (6) as $E_{\odot}(x, z) = E_{0,\odot}\tilde{E}_{\odot}(\tilde{x}, \tilde{z})$, using the same notation as in the previous sub-section. See Appendix 1 in the Supplementary Material for a discussion of the geometry of the image rings.

The total image charge, Q', is given by $Q' = -\frac{R}{\sqrt{A^2+d^2}}Q$ [4], and $L'_{\boxminus} = d'_2 - d'_1 = \frac{R^2}{A^2+(d+L_{\boxminus})^2}(d + L_{\boxminus}) - \frac{R^2}{A^2+d^2}d$.

Expanding to first order in $L_{\boxminus}$ gives $L'_{\boxminus} = \frac{(A^2-d^2)R^2}{(A^2+d^2)^2}L_{\boxminus}$. The closed form of $\frac{\partial E_{\boxminus}}{\partial z}$ is quite long to look at, but can be easily obtained and

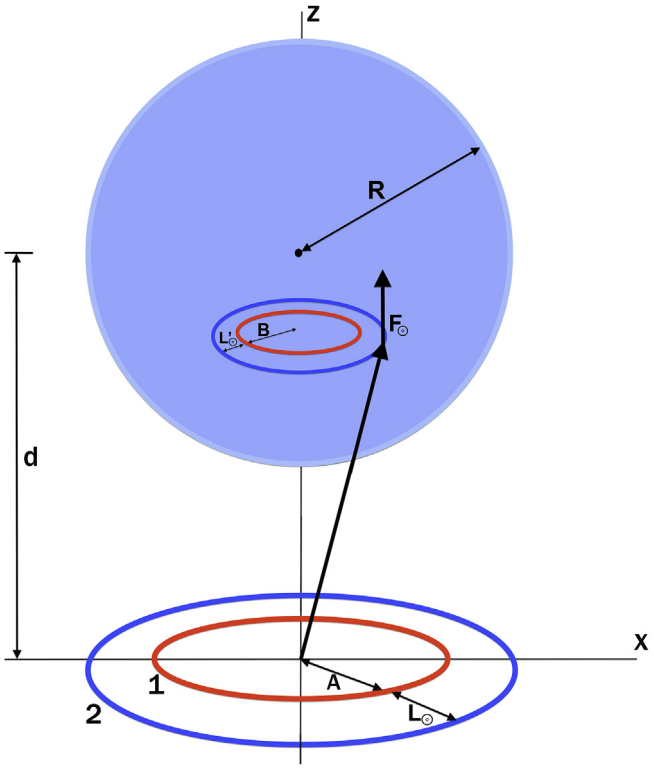

Fig. 3. Aerial side view of the concentric ring setup near an AFM tip, and the resulting image rings. The rings labeled "1" and "2" are of opposite charge, lying on the horizontal plane.

evaluated using symbolic programming languages [12] and Equation (5). With the above substitutions Equation (8) becomes

$$F_{\boxminus} = -F_{1,\boxminus}\left(\frac{\beta^2-\eta^2}{\left(\beta^2+\eta^2\right)^{\frac{5}{2}}}\right)\frac{\widetilde{\partial E_{\boxminus}}}{\partial z}, \tag{9}$$

where we used $\eta \equiv \frac{d}{R}$ and $\beta \equiv \frac{A}{R}$, and defined $F_{1,\boxminus} \equiv \frac{(QL_{\boxminus})^2}{(2\pi)^2 \varepsilon R^4} = \frac{p_{\boxminus}^2}{(2\pi)^2 \varepsilon R^4}$ as the unit of force, with $p_{\boxminus} = QL_{\boxminus}$ the dipole moment. At this point we evaluate $\frac{\widetilde{\partial E_{\boxminus}}}{\partial z}$ at $\tilde{x} = B/R = \frac{\beta}{\beta^2+\eta^2}$ and $\tilde{z} = \frac{d}{R} - \frac{d'}{R} = \eta - \frac{1}{\beta^2+\eta^2}\eta$ and multiply by 2π to obtain the vertical force on the entire image ring. This allows us to graph the dimensionless force $F_{\boxminus}/F_1$ vs. separation η for different values of ring size β (Fig. 4).

3.2. Force for the concentric case

The analysis for the concentric case is completely similar, except that we now take the derivative of the electric field with respect to x, since that is the direction in which the field on the image ring changes. Thus, the z-component of the force is

$$F_{\odot} = Q'\frac{\partial E_{\odot}}{\partial x}dx = Q'L'_{\odot}\frac{\partial E_{\odot}}{\partial x}. \tag{10}$$

As in §4.1, $L'_{\odot} = -\frac{(A^2-d^2)R^2}{(A^2+d^2)^2}L_{\odot}$. Following the above procedure yields the following expression for the force for the concentric configuration:

$$F_{\odot} = F_{1,\odot}\left(\frac{\beta^2-\eta^2}{\left(\beta^2+\eta^2\right)^{\frac{5}{2}}}\right)\frac{\widetilde{\partial E_{\odot}}}{\partial x}, \tag{11}$$

where $F_{1,\odot} \equiv \frac{(QL_{\odot})^2}{(2\pi)^2 \varepsilon R^4} = \frac{p_{\odot}^2}{(2\pi)^2 \varepsilon R^4}$. The graphic for the concentric case is qualitatively similar to the one shown in Fig. 4.

3.3. Force for the general ring orientation

Having determined the vertical force on an AFM tip exerted by rings in a concentric orientation or in a stacked one, we show here how to find that force for a pair of rings in an arbitrary, oblique configuration (Fig. 5). The electric field for such a system is found by adding the contributions from the concentric and the stacked cases, which gives

$$E = E_{\odot}\cos\phi + E_{\boxminus}\sin\phi, \tag{12}$$

where $E_{\odot}$ and $E_{\boxminus}$ are given by Equations (5) and (6), respectively, and ϕ is as shown in Fig. 5.

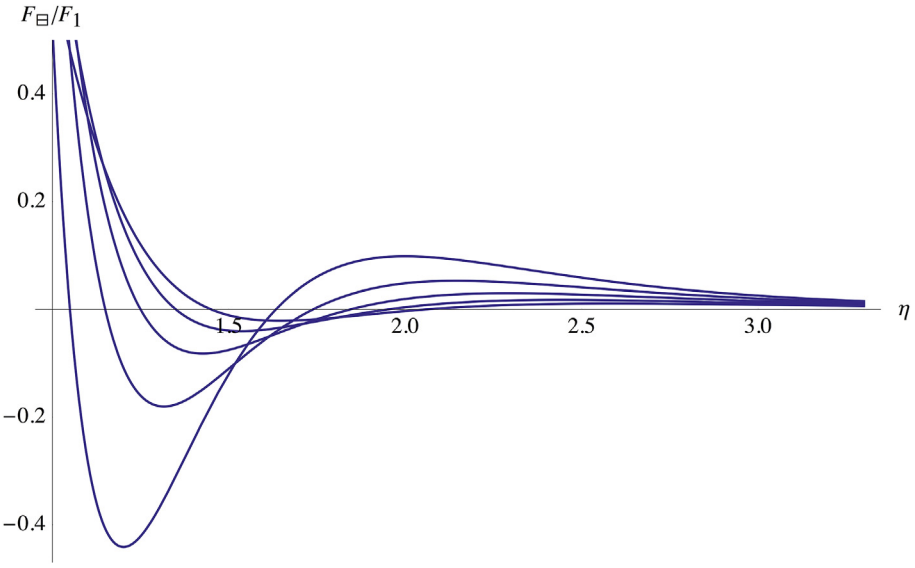

Fig. 4. $F_{\boxminus}/F_1$ vs. η for different values of β. The condition $\eta = 1$ represents the point of closest approach at which the tip and the substrate are in contact. The plots are for $1.05 < \beta < 1.45$, with β increasing in units of 0.1. The lowest value of β corresponds to the curve that dips lowest.

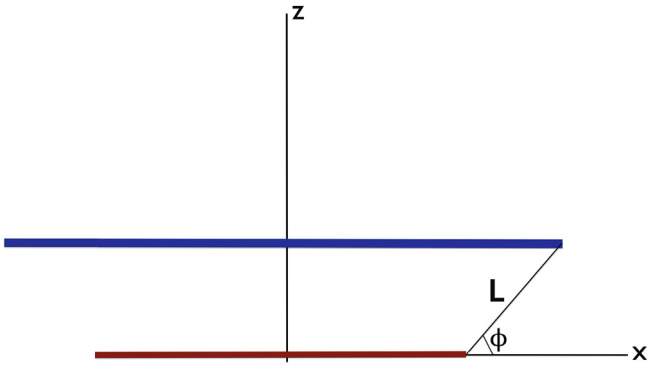

Fig. 5. Sagittal view of the original ring (lower, red ring) and one of the rings that constitute the shielding layer (top, blue) separated by a distance L at an angle ϕ. (For interpretation of the references to colour in this figure legend, the reader is referred to the web version of this article.)

Notice that $L_{\boxminus} = L\sin\phi$ and $L_{\odot} = L\cos\phi$, so we can eliminate $L_{\boxminus}$ and $L_{\odot}$ in Equations (5) and (6) in favor of the new variables, L and ϕ (Fig. 5).

Writing Equation (12) in differential form and multiplying throughout by $Q\prime$ we obtain the following,

$$F(\phi) = Q'dE = Q'dE_{\odot}\cos\phi + Q'dE_{\boxminus}\sin\phi \tag{13a}$$

of which the left side is the total force in the z-direction as a function of ϕ. Multiplying and dividing each term by the appropriate distance element, as done for Equation (8), we obtain

$$F(\phi) = Q'L'_{\odot}\frac{\partial E_{\odot}}{\partial x}\cos\phi + Q'L'_{\boxminus}\frac{\partial E_{\boxminus}}{\partial z}\sin\phi \tag{13b}$$

Now, from Equations (8) and (10) we have $F(\phi) = F_{\odot}\cos\phi + F_{\boxminus}\sin\phi$, where $F_{\boxminus}$ and $F_{\odot}$ are given by Equations (9) and (11), respectively. Substituting these last expressions yields

$$F(\phi) = F_1\left(\frac{\beta^2-\eta^2}{\left(\beta^2+\eta^2\right)^{\frac{5}{2}}}\right)\left(\frac{\widetilde{\partial E_{\odot}}}{\partial x}\cos^3\phi - \frac{\widetilde{\partial E_{\boxminus}}}{\partial z}\sin^3\phi\right), \tag{14}$$

where $F_1 \equiv \frac{(QL)^2}{(2\pi)^2\varepsilon R^4} = \frac{p^2}{(2\pi)^2\varepsilon R^4}$.

4. A practical application: ionic shielding in solution

As mentioned in the Introduction, these results can be used to model the effects of the shielding layer that develops around a ring sample in an ion-rich environment. A uniformly charged molecule placed in an electrolyte solution will attract oppositely charged ions, which will distribute themselves in a way that correlates with the geometry of the molecule.

To predict the force on the AFM tip that results from a shielded ring molecule, one may model the shielding layer as a superposition of many oppositely charged rings enveloping the original one. Because the ring is on a platform, the charges can only envelope it in a half torus, from 0 to π (Fig. 6).

In our model, the sample ring (red in Fig. 6) of total charge Q is surrounded by a shielding layer (blue) of total charge $-Q$. Now, while the ring has a linear charge density given by $\lambda = \frac{Q}{2\pi A}$, the charge of the shielding layer is distributed over the entire area of the half torus. Thus, assuming the charges are uniformly distributed, the shielding layer has a surface charge density, $\sigma = \frac{-Q}{2\pi^2 AL}$. The charge of a thin ring element of the half-toroidal shielding layer

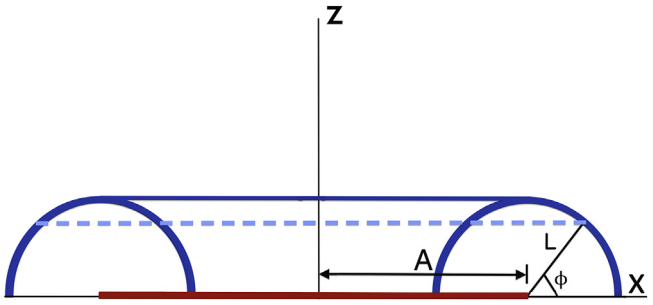

Fig. 6. Sagittal view of the ring and the counterionic shielding layer. The dotted light blue line represents a thin ring element of the half-toroidal shielding layer. (For interpretation of the references to colour in this figure legend, the reader is referred to the web version of this article.)

(dotted line in Fig. 6) is $dQ = 2\pi(A + L\cos\phi)\sigma L d\phi$.

To calculate the force, we use the *image* surface charge density $\sigma' = \frac{-Q'}{2\pi^2 BL'}$, where $B = \frac{AR^2}{A^2+d^2}$ and $L' = \frac{(A^2-d^2)R^2}{(A^2+d^2)^2}L$ (this can be confirmed by taking the vector sum of $L'_{\boxminus}$ and $L'_{\odot}$). A thin ring element of the image half-toroidal shielding layer is then

$$dQ' = 2\pi(B + L'\cos\phi)\sigma' L' d\phi, \tag{15}$$

Using Equation (13) we obtain an expression for the force differential:

$dF = \left(\frac{\partial E_{\odot}}{\partial x}L'_{\odot}\cos\phi + \frac{\partial E_{\boxminus}}{\partial z}L'_{\boxminus}\sin\phi\right)dQ\prime$. Substituting Equation (15), we integrate over ϕ from 0 to π, substitute the expressions for $L'_{\odot}, L'_{\boxminus}, \sigma'$, use $Q' = -\frac{R}{\sqrt{A^2+d^2}}Q$ [4], take out the dimensional terms of the electric field derivatives, $\frac{E_{0\boxminus}}{R} = \frac{QL_{\boxminus}}{(2\pi)^2\varepsilon R^4}$ and $\frac{E_{0\odot}}{R} = \frac{QL_{\odot}}{(2\pi)^2\varepsilon R^4}$, and simplify to obtain

$$F = F_1\frac{(A^2-d^2)R^3}{\pi\left(A^2+d^2\right)^{\frac{5}{2}}}\int_0^{\pi}\left(\frac{\widetilde{\partial E_{\boxminus}}}{\partial z}\sin^3\phi - \frac{\widetilde{\partial E_{\odot}}}{\partial x}\cos^3\phi\right)\left(1+\frac{L'}{B}\cos\phi\right)d\phi \tag{16}$$

$\frac{\widetilde{\partial E_{\boxminus}}}{\partial z}$ and $\frac{\widetilde{\partial E_{\odot}}}{\partial x}$ are not functions of ϕ and so may be taken out of the integral. For ions whose size is comparable to that of the charged ring (relevant in some cases), the distribution is discrete, and the integral Equation (16) can be converted into a summation, as given in Appendix 2 in the Supplementary Material. Distributing the integrand of Equation (16), separating and evaluating the integrals, and simplifying gives

$$F = F_1\frac{\beta^2-\eta^2}{\pi\left(\beta^2+\eta^2\right)^{\frac{5}{2}}}\left(\frac{4}{3}\frac{\widetilde{\partial E_{\boxminus}}}{\partial z} - \frac{3\pi}{8}\frac{\beta^2-\eta^2}{\beta^2+\eta^2}\frac{\tilde{L}}{\beta}\frac{\widetilde{\partial E_{\odot}}}{\partial x}\right) \tag{17}$$

where $\tilde{L\prime} \equiv \frac{L\prime}{R}$, $\tilde{\beta} \equiv \frac{B}{R} = \frac{AR}{A^2+d^2} = \frac{\beta}{\beta^2+\eta^2}$, and so $\frac{\widetilde{L\prime}}{\tilde{\beta}} = \frac{\beta^2-\eta^2}{(\beta^2+\eta^2)^2}\tilde{L}\frac{\beta^2+\eta^2}{\beta} = \frac{\beta^2-\eta^2}{\beta^2+\eta^2}\frac{\tilde{L}}{\beta}$.

As before, to obtain the force on the AFM tip, $\frac{\widetilde{\partial E_{\boxminus}}}{\partial z}$ and $\frac{\widetilde{\partial E_{\odot}}}{\partial x}$ in Equation (17) are evaluated at $\tilde{x} = B/R = \frac{\beta}{\beta^2+\eta^2}$ and $\tilde{z} = \frac{d}{R} - \frac{d'}{R} = \eta - \frac{1}{\beta^2+\eta^2}\eta$, and the resulting expression is multiplied by 2π. A step-by-step derivation of Equations (16) and (17) is given in Appendix 2 in the Supplementary Material.

Notably, one can use Equation (17) to estimate $\tilde{L} = \frac{L}{R}$, which is on the order of the Debye length [1,2], using experimental measurements of the force and after finding p as detailed in the Results section.

5. Results: measure size and dipole from AFM measurments

As seen in Fig. 4, for every value of ring radius β we have a curve that has two zero crossings, η_1 and η_2 (Fig. 7), for which $F_{\boxminus}/F_1 = 0$.

Notably, in all cases $\eta_1 = \beta$ exactly. This is because the term $\beta^2 - \eta^2$ appears in the numerator of all force expressions (Equations (9), (11), (14) and (17)). Therefore, one way to find the ring size is simply to find the first crossing. One starts with the tip touching the substrate and slowly pulls away until the force vanishes (cf. [4]). In practice, however, this may not always be feasible, and in such situations the initial distance from the platform is unknown.

In order to eliminate this unknown we find the second crossing, and subtract from it the first one. The distance between the crossings, $\eta_2 - \eta_1$, is a salient, experimentally determinable feature of the force-separation curve. Therefore, by finding the dependence of η_1 and η_2 on β, we can determine the size of the ring.

For the stacked case, the first crossing (blue line in Fig. 8) (in the web version) links the separation to the radius as $\eta_1 = \beta$, while the second crossing (red line) is given by $\eta_2 = 1.0758\beta + 0.5013$. Both equations were obtained numerically and are good to better than one part in a thousand. To find β we take $\eta_2 - \eta_1$ to obtain

$$\beta_{\boxminus} = \frac{\eta_2 - \eta_1 - 0.5013}{0.0758} \tag{18}$$

To find the dipole constant $p_{\boxminus}$ we first define $\frac{\eta_1+\eta_2}{2} \equiv \eta_{\boxminus,\, avg} = 1.0379\beta_{\boxminus} + 0.2507$, for which the force is strictly nonzero. Evaluating the force in Equation (9) at $\eta_{\boxminus,\, avg}$ and solving for $p_{\boxminus}$ gives

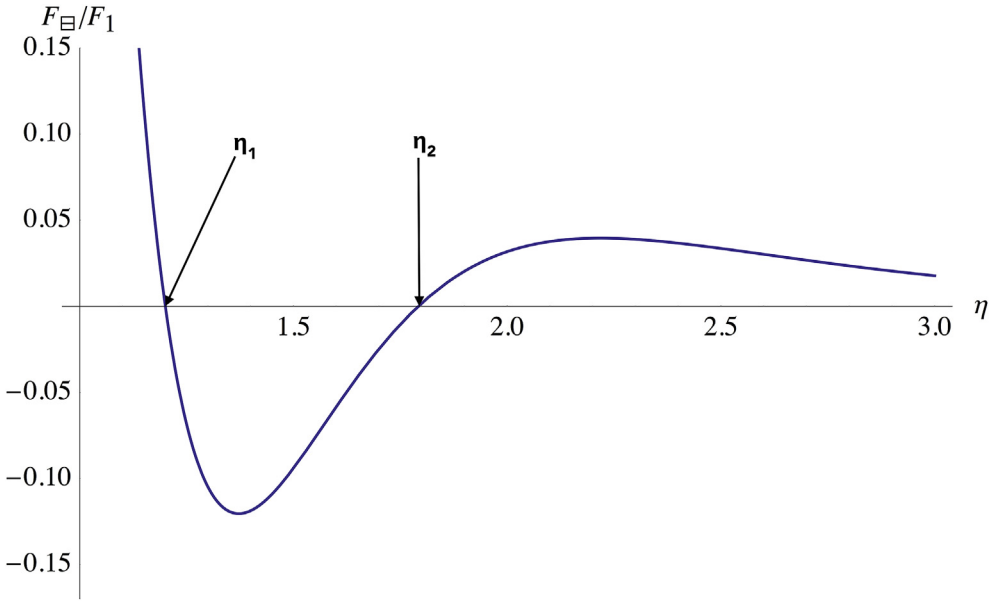

Fig. 7. Plot of $F_{\boxminus}/F_1$ vs. η for $\beta = 1.2$, showing the location of each crossing.

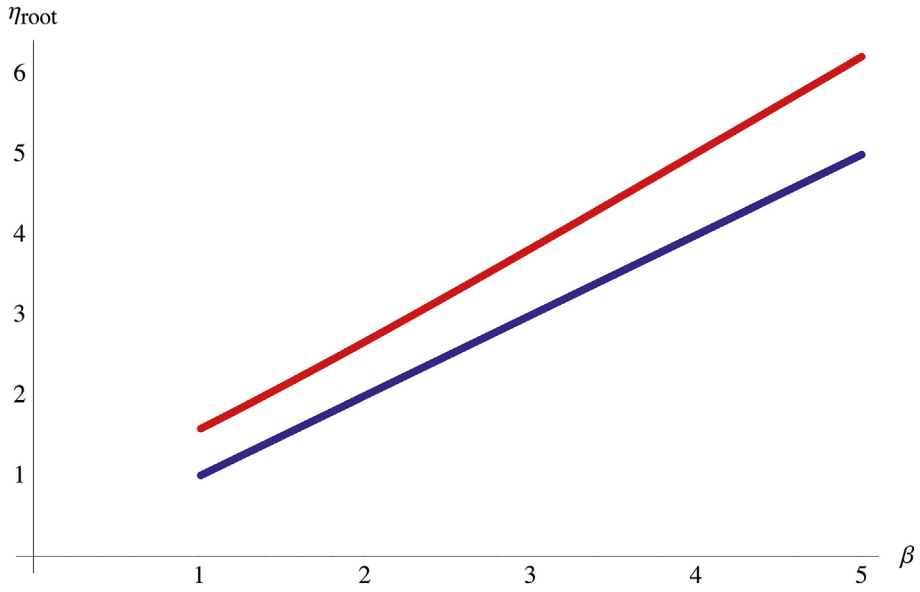

Fig. 8. Plots of the positions of the roots as a function of β. The blue line corresponds to η_1, while the red corresponds to η_2.

$$p_{\boxminus} = \sqrt{-(2\pi)^2 \varepsilon R^4 \frac{\left(\beta^2 + \eta_{\boxminus,avg}^2\right)^{\frac{5}{2}}}{\beta^2 - \eta_{\boxminus,avg}^2} \frac{F_{\boxminus}\left(\beta, \eta_{\boxminus,avg}\right)}{\left.\widetilde{\frac{\partial E_{\boxminus}}{\partial z}}\right|_{\eta=\eta_{\boxminus,avg}}}} \tag{19}$$

Using the same procedure for $F_{\odot}$ we find that $\eta_{2,\odot} = 0.6992\beta + 0.5380$, and so

$$\beta_{\odot} = \frac{0.5380 - (\eta_2 - \eta_1)}{0.3008} \tag{20}$$

$$\eta_{\odot,avg} = 0.8496\beta + 0.2690 \tag{21}$$

For the arbitrary ring configuration, $\eta_1(\beta, \phi) = \beta$, as before, and

$$\eta_2(\beta, \phi) = \eta_{2,\odot}, \cos^2\phi + \eta_{2,\boxminus}, \sin^2\phi,$$

which is accurate to within 5% for $0 \leq \phi \leq 2$. Substituting the expressions for $\eta_{2,\odot}$ and $\eta_{2,\boxminus}$ and solving for β, we obtain

$$\beta(\eta_2 - \eta_1, \phi) = \frac{\eta_2 - \eta_1 - 0.5380\cos^2\phi - 0.5013\sin^2\phi}{0.6992\cos^2\phi + 1.0758\sin^2\phi - 1} \tag{22}$$

and

$$\eta_{\phi,avg} = \left(0.3496\cos^2\phi + 0.5379\sin^2\phi + \frac{1}{2}\right)\beta + \left(0.2690\cos^2\phi + 0.2507\sin^2\phi\right) \tag{23}$$

For the whole shielding layer,

$$\beta = \frac{\eta_2 - \eta_1 - 0.6412}{0.0012} \tag{24}$$

and

$$\eta_{avg} = 1.0006\beta + 0.3206 \tag{25}$$

The equations for $p_{\odot}$, p_{ϕ} and p are derived as above for $p_{\boxminus}$, but starting instead from Equations (11), (14) and (18), respectively. These expressions are similar to Equation (19) and are given explicitly in Appendix 3 in the Supplementary Material. Notably, in all cases $\eta_1 = \beta$ exactly. This is because the term $\beta^2 - \eta^2$ appears in the numerator of all expressions.

6. Experimental studies of rings with AFM

Given the wide applicability of AFM in nanoscience, it is interesting to understand the experimental implications of the theoretical results presented here. Of particular relevance are extant experimental studies that use AFM to study ring structures immersed in liquid. We picked three such problems that span the length scales from hundreds of microns down to hundreds of $\mathring{A}$ from the following fields: inkjet printing ($10s\ \mu m$), molecular motors ($10s\ nm$) and light-harvesting bacteria ($100\mathring{A}$).

The charged droplets of inkjet printing have found lithographic applications for nano optoelectronics. In these uses a ubiquitous phenomenon appears: the coffee-ring formation, whereby a sediment ring is formed by the preferential motion of the particles in the droplet toward the periphery. These coffee rings have found applications in nanotransitor fabrication [13], in nanochromatography to separate small particles by size [14], and in transparent conductive coating [15]. In these three examples the tens-to-hundreds μm rings are successfully imaged with AFM. Given the charge content of these rings, and the charge shielding by the electrolytic solution or simply by the water in air humidity, the theoretical results presented here can serve to measure charge content in these structures.

One current approach to build molecular motors, as well as sensors and logical devises, is to use the self-assembly properties of DNA. In one such study interlocked rings of about 20 nm in diameter were built and measured with AFM [16]. The motor motion was correlated with the ambient pH, which in turn correlates with ionic surfactants.

Light-harvesting bacteria have been used as experimental models to understand the architecture and dynamics of photosynthesis. At the core of the process are proteins that act as antennas. These antennas have been found, via AFM, to have ring shapes with diameters in the $100\mathring{A}$ range [17]. Knowledge of charge content inside the rings should help to understand the ring interaction and the corresponding conformational assembly.

7. Conclusions

We have considered here several forces of interaction between rings of charge and AFM tips for several configurations. In the first case, a simple charged ring; in the second case, systems of charged rings of opposite charges. This second case was divided into two elemental cases, one in which the rings are on top of each other, and another in which the rings are coplanar. As a central application of these results, we considered a ring of charge dressed by oppositely charged ions originating in the embedding electrolyte. A central charge would be partially or fully balanced by the ions in solution, such that the observed force F_{obs} is a linear combination of the two extreme cases of no shielding and full shielding:

$$F_{obs} = (1 - \mathscr{S})F^0 + \mathscr{S}F, \tag{26}$$

where F^0 and F are given by Equations (4) and (17), respectively, and $\mathscr{S}$ is a constant, the shielding coefficient, such that $0 < \mathscr{S} < 1$. Further work can be conducted to determine the dependence of the shielding coefficient $\mathscr{S}$ on such factors as pH, pK_a, temperature, the presence of buffers, the degree of solvation, and ion density. Thus, the total force of the ring on the AFM tip mediated by a given electrolyte can be systematically studied using the expressions for the vertical force in this paper. The methods and results of this paper can not only be used to find the charge and size of rings in the various configurations described, but also to estimate the dimensionless Debye length by finding $\tilde{L}$, the distance from the sample ring to the shielding layer.

Acknowledgement

This project is funded by the National Science Foundation grant #CHE-1508085.

Appendix A. Supplementary data

Supplementary data related to this article can be found at http://dx.doi.org/10.1016/j.elstat.2017.05.004.

References

[1] H.-J. Butt, Electrostatic interaction in atomic force microscopy, Biophys. J. 60 (October 1991) 777–785.
[2] H.-J. Butt, Measuring local surface charge densities in electrolyte solutions with a scanning force microscope, Biophys. J. 63 (August 1992) 578–582.
[3] N. Mojarad, M. Krishnan, Measuring the size and charge of single nanoscale objects in solution using an electrostatic fluidic trap, Nat. Nanotechnol. 7 (July

2012), http://dx.doi.org/10.1038/NNANO.2012.99.
[4] D. Lazarev, F.R. Zypman, Determination of size and charge of rings by atomic force microscopy, J. Electrost. 83 (2016) 69.
[5] S. Hohlbauch, Nanomechanical and viscoelastic measurements in biological atomic force microscopy (AFM). Biophys. J. 110 (3) (498a–499a).
[6] G. Singh, K. Bremmellc, H.J. Griesserd, P. Kingshott, Colloid-probe AFM studies of the surface functionality and adsorbed proteins on binary colloidal crystal layers, RSC Adv. 7 (2017) 7329–7337, http://dx.doi.org/10.1039/C6RA28491D.
[7] T. Oliva, V. Tate, Q. Wen, K. Wang, K. Billiar, An inexpensive universal fluid cell for atomic force microscopy, in: 2014 40th Annual Northeast Bioengineering Conference (NEBEC), 2014, pp. 1–2, http://dx.doi.org/10.1109/NEBEC.2014.6972894. Boston, MA.
[8] M. Abramowitz, I.J. Stegun, Handbook of Mathematical Functions, National Bureau of Standards, vol. 55, AMS, 1964, 2nd printing.
[9] F.R. Zypman, Off-axis electric field of a ring of charge, Am. J. Phys. 74 (2006) 295, http://dx.doi.org/10.1119/1.2149869.
[10] G. Arfken, "Hypergeometric functions." §13.5, in: Mathematical Methods for Physicists, third ed., Academic Press, Orlando, FL, 1985, pp. 748–752.
[11] D. J. Griffiths, Introduction to Electrodynamics. fourth ed. Pearson Education, Inc. p. 171.
[12] Mathematica, Version 11.0, Wolfram Research, Inc., Champaign, IL, 2016.
[13] Y. Li, L. Lan, P. Xiao, S. Sun, Z. Lin, W. Song, E. Song, P. Gao, W. Wu, J. Peng, Coffee-ring defined short channels for inkjet-printed metal oxide thin-film transistors, ACS Appl. Mater. Interfaces 8 (2016) 19643–19648.
[14] T.-S. Wong, T.-H. Chen, X. Shen, C.-M. Ho, Nanochromatography driven by the coffee ring effect, Anal. Chem. 83 (2011) 1871–1873.
[15] M. Layani, M. Gruchko, O. Milo, I. Balberg, D. Azulay, S.M. agdassi, Transparent conductive coatings by printing coffee ring arrays obtained at room temperature, ACS Nano 3 (11) (2009) 3537–3542.
[16] T.L. Schmidt, A. Heckel, Construction of a structurally defined double-stranded DNA catenane, Nano Lett. 11 (2011) 1739–1742.
[17] S. Scheuring, F. Reiss-Husson, A. Engel, J.-L. Rigaud, J.-L. Ranck, High-resolution AFM topographs of Rubrivivax gelatinosus light-harvesting complex LH2, EMBO J. 20 (12) (2001) 3029–3035, http://dx.doi.org/10.1093/emboj/20.12.3029.